IEEE Open Journal of
Antennas and Propagation

Received 28 March 2021; revised 18 May 2021; accepted 22 May 2021. Date of publication 26 May 2021; date of current version 10 June 2021.

Digital Object Identifier 10.1109/OJAP.2021.3083938

VHF/UHF Ultrawideband Tightly Coupled Dipole Array for CubeSats

VIGNESH MANOHAR (Member, IEEE), SHUBHENDU BHARDWAJ (Member, IEEE), SATHEESH BOJJA VENKATAKRISHNAN (Senior Member, IEEE), AND JOHN L. VOLAKIS (Fellow, IEEE)

Department of Electrical and Computer Engineering, Florida International University, Miami, FL 33199, USA

CORRESPONDING AUTHOR: V. MANOHAR (e-mail: vmanohar@fiu.edu)

This work was supported by the Air Force Office of Scientific Research under Grant FA9550-19-1-0290.

ABSTRACT To date, CubeSat radars and imagers have been limited to operations beyond S-band due to the challenges associated with the design of wideband, compact, low-frequency antennas. Concurrently, the frequencies at VHF/UHF bands can image through clouds and foliage, and are very attractive for ice, water and biomass sensing. There is thus a need to develop wideband antennas that can operate at VHF/UHF bands which are low cost, light-weight, and packable. In this paper, we present a CubeSat deployable Tightly Coupled Dipole Array (TCDA) that achieves VSWR$<$3 from 80 MHz - 600 MHz, and VSWR$<$4 from 65 MHz - 600 MHz. While the array itself is 1.2 m in length, 10 cm in width and 1.5 mm in thickness, it can be folded and stowed in a compact volume of 0.40U. We detail the design of the array, demonstrate the folding mechanism, and validate its performance through measurements.

INDEX TERMS CubeSats, VHF/UHF antennas, ultrawideband antennas, satellite antennas.

I. INTRODUCTION

CUBESATS represent a class of miniaturized satellites that can weigh as little as 1.33 kg and occupy a volume of $10 \times 10 \times 10$ cm^3 (commonly referred to as 1U). Due to their small sizes, light-weight, and low development costs, CubeSat missions are rapidly growing. The low-costs associated with CubeSat development enable the vision of a constellation of synchronized CubeSats in space, thereby opening doors to missions that were deemed impossible with conventional satellites. From a remote sensing and imaging perspective, CubeSat constellations offer the potential of synthesizing an electrically large aperture in space to provide narrow beams for high resolution imaging. This is especially relevant for lower frequencies where an antenna aperture of hundreds of meters is required to get reasonable resolution from a 400 km Low Earth Orbit. While Synthetic Aperture Radar (SAR) techniques can be used to generate a large aperture in the direction of motion of the satellite (along-track), reasonable resolution in the cross-track at low frequencies can only be achieved through a constellation of CubeSats [1], [2]. Apart from this, the constellation concept improves the reliability of the satellite system since a single CubeSat failing does not lead to mission failure. As such, a replacement CubeSat can be readily piggy-backed on a future mission.

Presently, several earth science missions with CubeSats are evolving at S-band and above [3]. Examples include the RainCube mission at Ka-band for precipitation sensing [4], [5] and CIRES mission at S-band, which is space-based interferometric SAR to detect changes to the Earth's biomass and land profile [3], [6]. Many other missions for CubeSat constellation based SAR are reviewed in [2]. However, VHF/UHF bands for CubeSat based radar imaging have not yet been pursued due to the requirement of large antenna apertures. Concurrently, VHF/UHF frequencies are attractive for sensing ice thickness [7], soil moisture [8], vegetation biomass, and for exploring the nature of asteroids in our solar system [9]. Additionally, these frequencies can achieve greater propagation depths and penetrate through dense foliage [10]. Further, the range resolution for a radar is inversely proportional to the bandwidth of the transmitted signal [2]. Thus, there is a need to equip CubeSats with VHF/UHF ultrawideband deployable antennas thereby enabling constellation-based, high resolution imaging.

While several antenna designs for CubeSats have evolved with time [11]–[13], dipole antennas are the most common

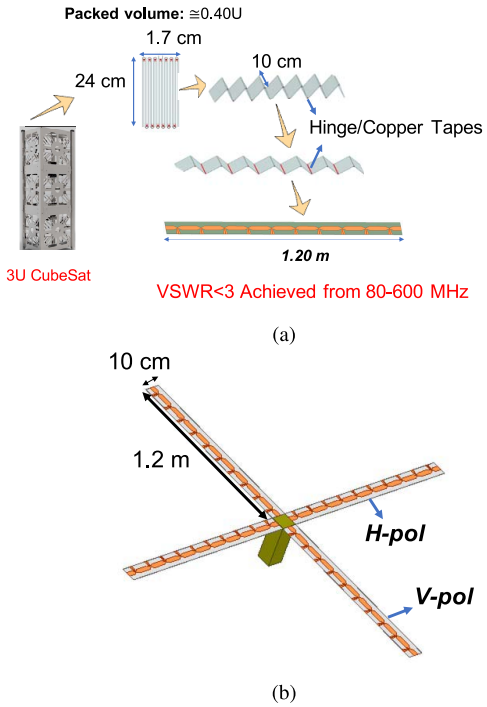

FIGURE 1. Artist illustration of the wideband VHF/UHF Tightly Coupled Dipole Array and its integration with a 3U CubeSat. (a) Folding and deployment sequence, and (b) Illustration of 4 arrays with a combined volume under 2U for dual-polarized and circularly polarized applications.

at VHF/UHF frequencies [14]–[18]. They are typically, wrapped around the satellite during launch, and deployed using their stored mechanical energy (akin to a tape measure) [19]. However, their dipole-like resonance severely limits bandwidth performance, thereby inhibiting wideband imaging. Reflector antennas have already demonstrated their potential for CubeSat missions at S-band and above [4], [20]. However, they become unmanageably large at VHF/UHF frequencies. Patch arrays, on the other hand, are narrowband and have large $\lambda/2$ size elements [21]. Therefore, for low-frequency and wideband applications, they are not a suitable choice.

In contrast to the above, this work proposes an antenna which is compact, easily foldable, very thin and wideband (>7:1). The antenna is based on the established theory of connected dipole arrays [22], and the wider bandwidth Tightly Coupled Dipole Arrays (TCDA) [23], [24]. To conform to the mechanical constraints of CubeSats, this paper describes the design of a linear version of the TCDA. The presented design has a total length of 1.2 m ($\lambda/3$ at 80 MHz), a width of 10 cm and a thickness of 1.5 mm as shown in Fig. 1. It should be noted that only the center elements of the array are excited to achieve the wide bandwidth. Upon folding, it can fit in a 0.40U volume as shown in Fig. 1. Folding of the array is demonstrated by connecting its elements with copper tapes. The designed TCDA can be integrated within a 3U/6U CubeSat, and enable low-frequency operation. Notably, four such 1.2 m long TCDAs can be integrated within a 2U volume to enable dual-polarized or circularly polarized imagers (see Fig. 1b).

II. DESIGN OF WIDEBAND VHF/UHF TIGHTLY COUPLED DIPOLE ARRAY

A. INFINITE ARRAY DESIGN

The TCDA's design was carried out by optimizing the unit cell to achieve wideband performance in an infinite array setting [25]. A 1.5 mm thick Rogers RO3003 substrate was chosen, having an $\epsilon_r = 3$, and $\tan\,\delta = 0.001$. To model a differential port formed by the pair of 50 Ω connectors attached to each dipole arm, a 100 Ω lumped port is used to excite the unit cell as shown in Fig. 2a [26]. Notably, the width of the unit cell was 10 cm, chosen to comply with CubeSat chassis dimension. Further, the overall array length was chosen so that the desired bandwidth is achieved. It is also remarked that our design does not include a ground plane. Thus, there is no need to concurrently optimize the inductance and capacitance of the unit cell using overlapping dipoles or metal inserts [23], [27].

The resulting active VSWR for the final unit cell design, shown in Fig. 2a, is given in Fig. 2b. Clearly, the infinite array has very good matching across the entire band of 60 MHz - 600 MHz. The simplicity of this unit cell makes it very attractive for CubeSats. Specifically, the single-sided PCB design makes it low cost and light-weight. As such, the design lends itself to textile implementations for further packability [24]. Notably, the differential feed employed by our design enables high dynamic range and low-noise operations [28]. This also allows the antenna to directly interface with differential amplifiers without the need for a balun, thereby reducing hardware requirements aboard the CubeSat.

B. FINITE ARRAY SIMULATIONS

Using the unit cell design described in Section II-A, we proceed to present a finite array design suitable for a CubeSat form factor. Notably, the space constraints do not allow for a 2-D array typical of TCDA implementations. This implies a smaller bandwidth for the 1D array [29]. To achieve the desired wideband performance with a linear array implementation, two factors are critical: (a) number of unit cells, and (b) the number of ports being excited/terminated with a 100 Ω port impedance. Further, to fit the array within a 0.5U volume, the length should be no more than 1.2 m. Thus, 10 unit cells were chosen to form the 1D array. The even number of ports result in two center elements that can be excited. This results in significant coupling to improve low-frequency performance. The design of the final finite array is shown in Fig. 3. If a longer array is chosen, more ports could potentially be excited allowing for beam steering. As with the unit cell simulations, a 100 Ω lumped port was placed in between the dipole arms.

The active as well as passive S-parameters for the center ports (labeled as ports 5 and 6 in Fig. 3a) are shown in Fig. 3. It is important to note that the passive reflection coefficient shows poor impedance matching at lower

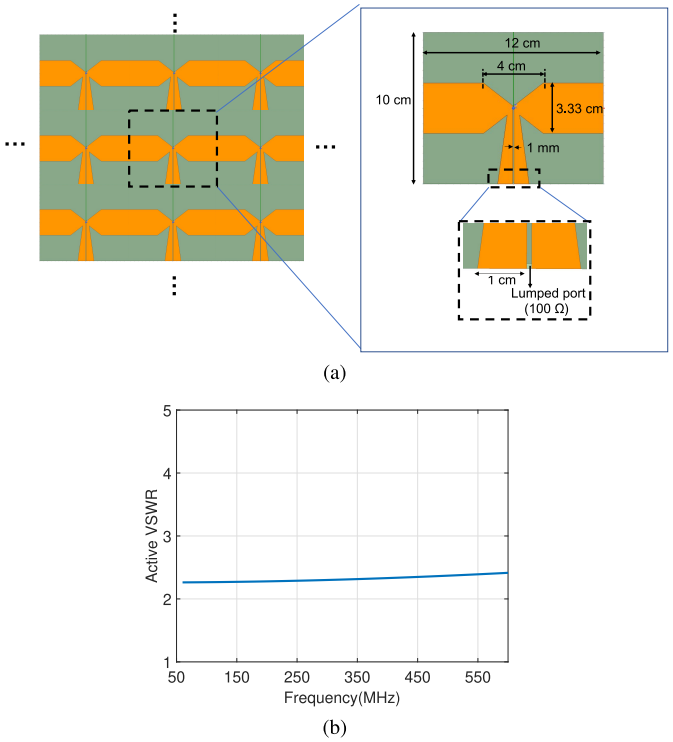

FIGURE 2. VSWR simulations of a TCDA in an infinite array setting. (a) Unit cell dimensions and (b) active VSWR.

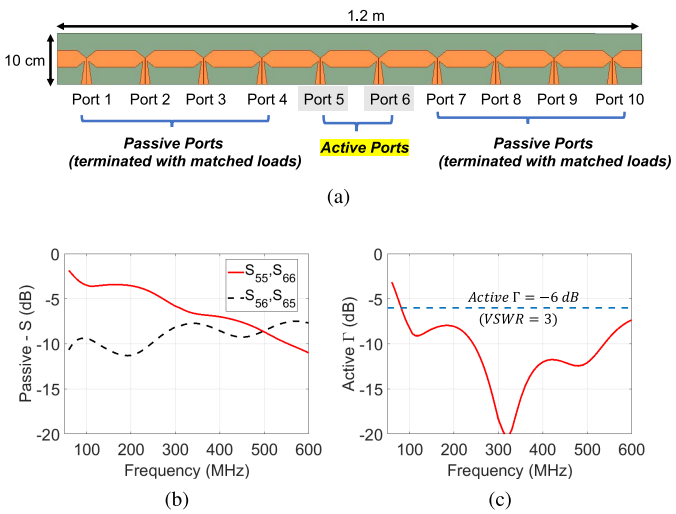

FIGURE 3. Ten-element finite array simulations. (a) Illustration of the tightly coupled dipole array employing 10 unit cells out of which ports 5 and 6 are active. (b) Passive S-parameter vs frequency and (c) active reflection coefficient for the center element(s). The active reflection coefficient is under −6 dB across 80 MHz - 600 MHz.

frequencies. However, when both center ports are excited equally, the coupling between these ports (accounted for in the active reflection coefficient [30]) lead to significant improvement in the reflection coefficient.

The simulated E-plane radiation patterns are shown in Fig. 4, and the peak directivities and realized gain values are shown in Table 1. We remark here that the cross-pol levels for the array are well under −30 dB. As expected,

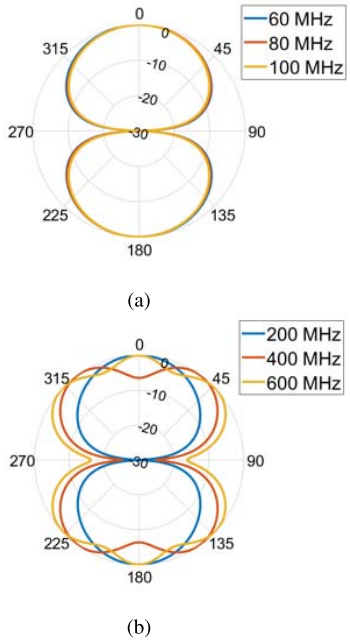

FIGURE 4. Simulated normalized E-plane radiation patterns of the 10-unit cell finite TCDA at (a) 60, 80 and 100 MHz and (b) 200, 400 and 600 MHz. The peak values are provided in Table 1.

above 250 MHz, the pattern begins to deviate from the ideal dipole pattern. This is because the array length is greater than 1λ [24]. The realized gain remains greater than −10 dB between 80 MHz - 600 MHz. Notably, the reduced efficiency at the lower frequencies is a manifestation of the strong coupling between the dipoles to ensure good matching across the band. A more comprehensive description of the relation between efficiency and coupling between dipoles is given later in Section III-B. Of course, the constellation gain can be increased by adding more CubeSats. However, the low VSWR of individual elements ensures minimal power return, implying that a single antenna module can possibly be used for transmission and reception, further reducing hardware requirements. Additionally, constellation-level beam forming can be accomplished by controlling the amplitude and phase of each CubeSat.

III. ARRAY FABRICATION AND MEASUREMENTS

A. FABRICATION

To verify the designed VHF/UHF array, the 10-unit cell TCDA was fabricated using 5 foldable RO3003 substrate sections, with each consisting of 2 unit cells as shown in Fig. 5. The copper on the opposite side of the board was completely etched out. As depicted, the folding was achieved using copper tapes at the unit cell boundaries. Notably, low-profile hinges can be used in conjunction with these copper tapes for improved mechanical stability.

The proposed accordion-like folding of the array is shown in Fig. 5b, with the stowed array in Fig. 5c. Since two unit cells were fabricated on a single section, the dimensions of the stowed array (along with connectors) are

TABLE 1. Simulated directivity and realized gain for the finite TCDA consisting of 10 unit cells as a function of frequency.

Frequency (Wavelength)	Electrical Length	Directivity (dB)	Realized Gain (dB)
60 MHz (5m)	0.24λ	2.24	-12.66
80 MHz (3.75m)	0.32λ	2.26	-8.98
100 MHz (3m)	0.40λ	2.35	-6.82
200 MHz (1.5m)	0.80λ	2.90	-3.64
400 MHz (0.75m)	1.60λ	2.74	-1.42
600 MHz (0.5m)	2.40λ	2.00	-1.03

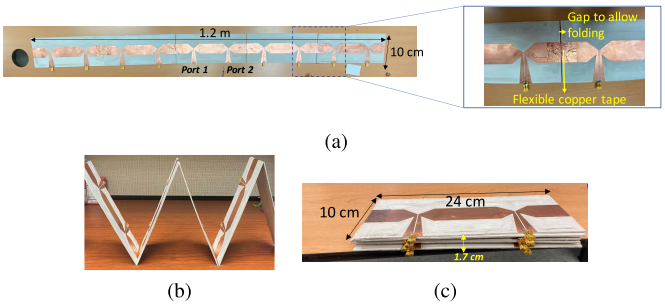

FIGURE 5. (a) Fabricated prototype of the wideband VHF/UHF TCDA. Copper tapes were placed between sections to ensure electrical continuity and facilitate folding; (b) Intermediate stage of deployment; (c) Completely stowed array with a volume of 0.408U.

24 cm×10 cm×1.7 cm, implying a volume of 408 cm^3 (0.408U). As such, this array can be directly integrated into a 3U CubeSat chassis. A 50 Ω sub miniature push-on micro (SMPM) connector was placed at the end of each dipole arm, resulting in a 100 Ω differential impedance [26]. Indeed, the low-profile of the SMPM connectors ensures compact volume for the stowed array.

B. MEASUREMENT RESULTS

To measure the S-parameters of the fabricated array, a 4-port Vector Network Analyzer (VNA) was configured for the differential mode feed. Specifically, a pair of ports were used to serve as an ideal 180° hybrid coupler to measure the balanced S-parameters at each dipole [28]. First, the differential S-parameters for the two center dipoles were recorded and processed to compute the active VSWR at each port (see Fig. 6). It is evident that a very good match is achieved between measured and simulated VSWR curves. The measured array achieves VSWR<3 across a 7.5:1 bandwidth (80 MHz - 600 MHz) and VSWR<4 across a 9:1 bandwidth (65 MHz - 600 MHz).

1) ARRAY EFFICIENCY

Due to difficulties associated with the low frequency measurements, we considered an alternate approach for efficiency characterizations. Assuming that the loss in the substrates are negligible, any loss of efficiency is due to the power coupled between the ports. Thus, the ratio between the coupled power and the input power will be termed as 'decoupling efficiency, $\eta_{decoupling}$'. The latter is given by the expression [31], [32]:

$$\eta_{decoupling} = 1 - \frac{P_{coupled}}{P_{incident}} = 1 - \frac{\sum_{n=1}^{N} |b_n|^2}{\sum_{m=1}^{M} |a_m|^2} \quad (1)$$

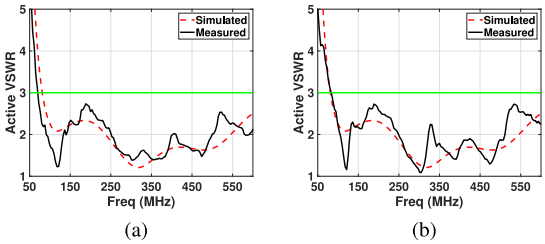

FIGURE 6. Comparison between simulated and measured active reflection coefficient at (a) port 5 and (b) port 6 of the fabricated TCDA. Refer to Fig. 3 for port numbering.

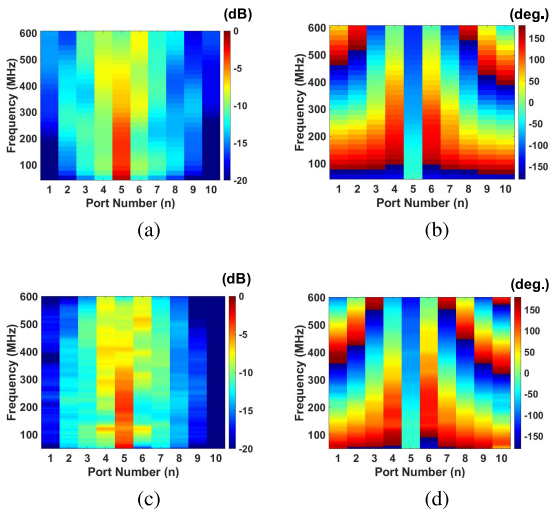

FIGURE 7. Passive S-parameters with port 5 excited (S_{n5}) as a function of frequency: (a) Simulated amplitude; (b) Simulated phase; (c) Measured amplitude; (d) Measured phase.

where $|a_m|^2$ and $|b_n|^2$ represent the powers entering the m^{th} port and leaving the n^{th} port, respectively. These coefficients are related via the S-parameters as [33]

$$b_n = \sum_{m=1}^{M} S_{nm} a_m \quad (2)$$

For our array, we only excited the center 2 elements (ports 5 and 6). It is thus required to measure the S-parameters: $S_{1,5}, S_{2,5}, \ldots, S_{10,5}$ and $S_{1,6}, S_{2,6}, \ldots, S_{10,6}$. Notably, the symmetry in the design allows us to only measure coupling terms related to port 5.

The variation of the measured S-parameter values as a function of frequency and port-number is given in Fig. 7. Indeed, a reasonable agreement is seen between the measured and simulated values. These measured values were then substituted in (1) to extract the efficiency. We also calculated the simulated efficiency using the ratio of the realized gain to directivity (identical values are obtained when simulated S-parameters are substituted in (1)). A comparison between the simulated and measured efficiency is provided in Fig. 8, where a reasonable match is seen between them. The variations observed at lower frequencies are due to interference

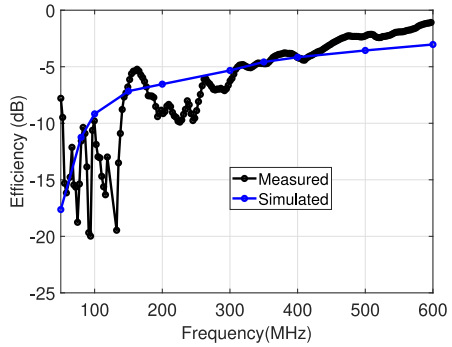

FIGURE 8. Comparison between simulated and measured efficiency of the 10-element TCDA.

effects, possibly caused by the finite array and nearby reflections. These results illustrate that the designed array achieves the broadband impedance matching through coupling. We anticipate that a 2D array will achieve higher efficiencies. However, the mechanical complexity of such a design makes it less attractive for CubeSats. As noted earlier, the effective gain can always be increased by adding more CubeSats to the constellation.

IV. SIMULATION ANALYSIS OF FOUR TCDAS ON A 3U CUBESAT

In this section, we provide simulations to illustrate the potential of employing four VHF/UHF ultrawideband TCDAs for dual-polarized CubeSat imaging. The configuration is shown in Fig. 9, assuming a 3U CubeSat chassis ($10\times10\times30$ cm^3). As noted, the four TCDAs can be stowed in under 2U volume. For x polarization, feed 1 and feed 2 are excited, whereas for y polarization, feed 3 and feed 4 are excited. Note that each feed consists of two ports, as described previously.

The active VSWR (at each port), and the decoupling efficiency are given in Fig. 10. It is evident that the bandwidth of operation (VSWR$<$3 for 80 MHz - 600 MHz) is retained for all the four TCDAs. Notably, for frequencies under 100 MHz ($\lambda = 3$ m), the separation between the TCDAs is less than $\lambda/2$. Thus, the two TCDAs (that deliver either x or y polarization) Radiate as a single large TCDA, leading to improved efficiencies. For frequencies above 100 MHz, the efficiency of the four TCDAs match those of the single TCDA, implying a reduction in coupling between them. From Fig. 10, we can also remark the VSWR/efficiency for x and y polarizations are practically identical.

The radiation patterns at 200 MHz for the 4-TCDAs are shown in Fig. 11. Ludwig's 3rd definition was used to compute the x and y components of the fields (denoted as L3X and L3Y) [34]. As expected, the cross pol for each polarization is well under -30 dB, implying good isolation. The peak total directivity and realized gain as a function of frequency for each polarization is tabulated in Table 2. Cearly, the directivity and gain increase significantly beyond 100 MHz compared to a single TCDA (see Table 1). However, for

TABLE 2. Simulated peak directivity and realized gain as a function of frequency for 4 TCDAs mounted on a 3U CubeSat.

Frequency (Wavelength)	x-polarized mode		y-polarized mode	
	Directivity (dB)	Realized Gain (dB)	Directivity (dB)	Realized Gain (dB)
60 MHz (5 m)	2.79	-9.41	2.82	-9.38
80 MHz (3.75 m)	3.31	-6.05	3.34	-6.00
100 MHz (3 m)	3.82	-4.10	3.76	-4.16
200 MHz (1.5 m)	5.82	-0.57	5.85	-0.53
400 MHz (0.75 m)	5.50	1.44	5.50	1.45
600 MHz (0.5 m)	5.13	2.09	5.14	2.10

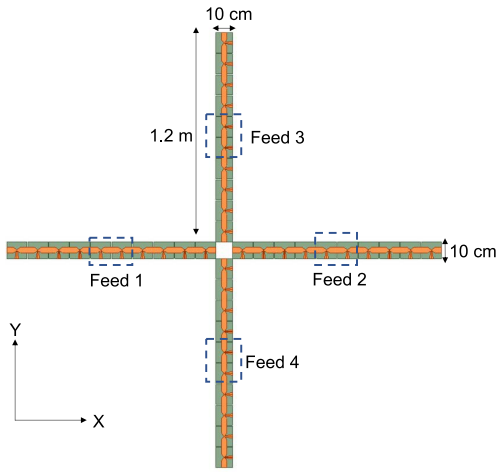

FIGURE 9. Simulation setup of the 4 wideband VHF/UHF TCDAs placed on a 3U (10x10x30 cm^3) CubeSat chassis.

frequencies above 230 MHz, the separation between the centers of the individual TCDAs exceeds a wavelength, implying multiple sidelobes in the radiation pattern. This issue can be circumvented if only one TCDA per polarization is used beyond 230 MHz. Of course, the tradeoff here is the low directivity for a single TCDA, necessitating a larger constellation to achieve the same gain.

V. CONCLUSION

This paper presented a VHF/UHF ultrawideband deployable array for CubeSats. The array achieves VSWR$<$ 3 between 80 MHz - 600 MHz, and VSWR$<$4 between 65 MHz - 600 MHz. The dimensions of the deployed array are 1.2 m$\times$10 cm$\times$1.5 mm. Folding was achieved by discretizing the design into 5 sections, and connecting them via copper tapes. We remark that any other flexible conductor can be used in lieu of copper tapes. On folding, the volume of the array is $24\times10\times1.7$ cm^3, implying a stowed volume of 0.408U. As such, the array is attractive for CubeSats. The compact stowed volume makes it possible to pack four such antennas within a 2U volume, thereby enabling a dual polarized/circularly polarized operation. The performance of the antenna was validated through measurements. In the future, low-profile hinges along with space-qualified materials will be considered.

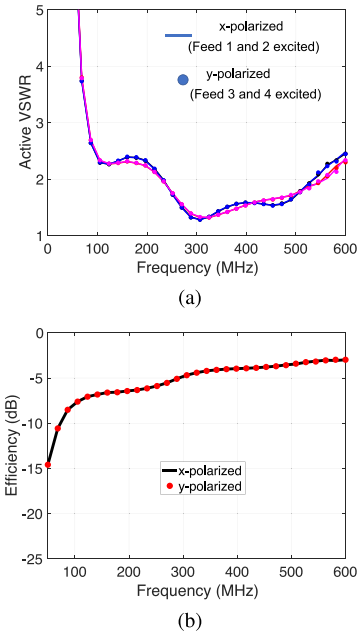

FIGURE 10. (a) Active VSWR at ports shown in Fig. 9. Note that all the ports have VSWR<3 across 80 MHz-600 MHz. (b) Plot of the decoupling efficiency using (1).

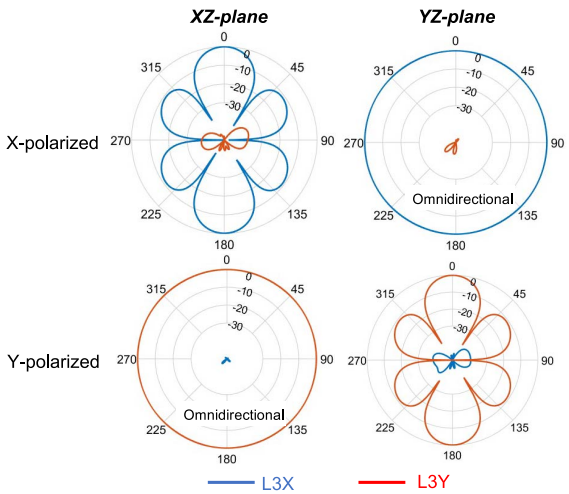

FIGURE 11. Radiation patterns of the dual polarized TCDA at 200 MHz. The peak values are tabulated in Table 2.

ACKNOWLEDGMENT

The authors would like to thank Malcolm Taaffe and Md. Rakibul Islam for their help in fabricating and measuring the antennas.

REFERENCES

[1] P. Gogineni *et al.*, "A CubeSat train for radar sounding and imaging of antarctic ice sheet," in *Proc. IEEE Int. Geosci. Remote Sens. Symp.*, Valencia, Spain, 2018, pp. 4138–4141.

[2] S. W. Paek, S. Balasubramanian, S. Kim, and O. de Weck, "Small-satellite synthetic aperture radar for continuous global biospheric monitoring: A review," *Remote Sens.*, vol. 12, p. 2546, Aug. 2020.

[3] E. Peral *et al.*, "Radar technologies for earth remote sensing from CubeSat platforms," *Proc. IEEE*, vol. 106, no. 3, pp. 404–418, Mar. 2018.

[4] N. Chahat, R. E. Hodges, J. Sauder, M. Thomson, E. Peral, and Y. Rahmat-Samii, "CubeSat deployable Ka-band mesh reflector antenna development for earth science missions," *IEEE Trans. Antennas Propag.*, vol. 64, no. 6, pp. 2083–2093, Jun. 2016.

[5] Y. Rahmat-Samii, V. Manohar, J. M. Kovitz, R. E. Hodges, G. Freebury, and E. Peral, "Development of highly constrained 1 m Ka-band mesh deployable offset reflector antenna for next generation CubeSat radars," *IEEE Trans. Antennas Propag.*, vol. 67, no. 10, pp. 6254–6266, Oct. 2019.

[6] *New NASA Radar Looks to Monitor Volcanoes and Earthquakes From Space*. Accessed: Feb. 15, 2021. [Online]. Available: https://www.nasa.gov/feature/goddard/2020/new-nasa-radar-looks-to-monitor-volcanoes-and-earthquakes-from-space

[7] C. Lewis *et al.*, "Airborne fine-resolution UHF radar: An approach to the study of englacial reflections, firn compaction and ice attenuation rates," *J. Glaciol.*, vol. 61, no. 225, pp. 89–100, 2015.

[8] M. Moghaddam *et al.*, "Microwave observatory of subcanopy and subsurface (MOSS): A mission concept for global deep soil moisture observations," *IEEE Trans. Geosci. Remote Sens.*, vol. 45, no. 8, pp. 2630–2643, Aug. 2007.

[9] *Hera's CubeSat to Perform First Radar Probe of an Asteroid*. Accessed: Feb. 15, 2021. [Online]. Available: https://www.esa.int/Safety_Security/Hera/Hera_s_CubeSat_to_perform_first_radar_probe_of_an_asteroid

[10] Y. S. Meng, Y. H. Lee, and B. C. Ng, "Study of propagation loss prediction in forest environment," *Progr. Electromagn. Res. B*, vol. 17, pp. 117–133, Aug. 2009.

[11] Y. Rahmat-Samii, V. Manohar, and J. M. Kovitz, "For satellites, think small, dream big: A review of recent antenna developments for CubeSats," *IEEE Antennas Propag. Mag.*, vol. 59, no. 2, pp. 22–30, Apr. 2017.

[12] R. L. Baktur, "Antennas for CubeSats," in *Antenna Engineering Handbook*, 5th ed., J. L. Volakis, Ed. New York, NY, USA: McGraw-Hill, 2018, ch. 41.

[13] S. Gao *et al.*, "Antennas for modern small satellites," *IEEE Antennas Propag. Mag.*, vol. 51, no. 4, pp. 40–56, Aug. 2009.

[14] X. Zhang, F. Sun, G. Zhang, and L. Hou, "Compact UHF/VHF monopole antennas for CubeSats applications," *IEEE Access*, vol. 8, pp. 133360–133366, 2020.

[15] T. F. C. Leao, V. Mooney-Chopin, C. W. Trueman, and S. Gleason, "Design and implementation of a diplexer and a dual-band VHF/UHF antenna for nanosatellites," *IEEE Antennas Wireless Propag. Lett.*, vol. 12, pp. 1098–1101, 2013.

[16] K. Schraml, A. Narbudowicz, S. Chalermwisutkul, D. Heberling, and M. J. Ammann, "Easy-to-deploy LC-loaded dipole and monopole antennas for CubeSat," in *Proc. 11th Eur. Conf. Antennas Propag. (EUCAP)*, Paris, France, 2017, pp. 2303–2306.

[17] M. Deshpande and J. Piepmeier. *Design and Development of VHF Antennas for Space Borne Signal of Opportunity Receivers for Cubesat Platforms*. Accessed: 2015. [Online]. Available: http://ntrs.nasa.gov/

[18] W. Alomar, J. Degnan, S. Mancewicz, M. Sidley, J. Cutler, and B. Gilchrist, "An extendable solar array integrated Yagi-Uda UHF antenna for CubeSat platforms," in *Proc. IEEE Int. Symp. Antennas Propag.*, Spokane, WA, USA, 2011, pp. 3022–3024.

[19] J. Costantine, Y. Tawk, C. G. Christodoulou, J. Banik, and S. Lane, "CubeSat deployable antenna using bistable composite tape-springs," *IEEE Antennas Wireless Propag. Lett.*, vol. 11, pp. 285–288, 2012.

[20] M. Aherene, T. Barrett, L. Hoag, E. Teegarden, and R. Ramadas, "Aeneas—Colony I meets three-axis pointing," in *Proc. 25th Annu. AIAA/USU Conf. Small Satellites*, 2011, pp. 1–11.

[21] D. R. Jackson, "Microstrip antennas," in *Antenna Engineering Handbook*, 5th ed., J. L. Volakis, Ed. New York, NY, USA: McGraw-Hill, 2018.

[22] D. Cavallo, "Connected array antennas: Analysis and design," Ph.D. dissertation, Dept. Elect. Eng., Technische Universiteit Eindhoven, Eindhoven, The Netherlands, 2011, doi: 10.6100/IR719461.

[23] I. Tzanidis, K. Sertel, and J. L. Volakis, "UWB low-profile tightly coupled dipole array with integrated balun and edge terminations," *IEEE Trans. Antennas Propag.*, vol. 61, no. 6, pp. 3017–3025, Jun. 2013.

[24] J. Zhong, C. W. Lee, D. Papantonis, A. Kiourti, and J. L. Volakis, "Body-worn 30:1 bandwidth tightly coupled dipole array on conductive textiles," *IEEE Antennas Wireless Propag. Lett.*, vol. 17, no. 5, pp. 723–726, May 2018.

[25] T. F. Eibert, J. L. Volakis, D. R. Wilton, and D. R. Jackson, "Hybrid FE/BI modeling of 3-D doubly periodic structures utilizing triangular prismatic elements and an MPIE formulation accelerated by the Ewald transformation," *IEEE Trans. Antennas Propag.*, vol. 47, no. 5, pp. 843–850, May 1999.
[26] D. E. Bockelman and W. R. Eisenstadt, "Combined differential and common-mode scattering parameters: Theory and simulation," *IEEE Trans. Microw. Theory Techn.*, vol. 43, no. 7, pp. 1530–1539, Jul. 1995.
[27] J. P. Doane, K. Sertel, and J. L. Volakis, "A wideband, wide scanning tightly coupled dipole array with integrated balun (TCDA-IB)," *IEEE Trans. Antennas Propag.*, vol. 61, no. 9, pp. 4538–4548, Sep. 2013.
[28] A. D. Johnson, V. Manohar, S. B. Venkatakrishnan, and J. L. Volakis, "Optimized differential TCDA (D-TCDA) with novel differential feed structure," *IEEE Open J. Antennas Propag.*, vol. 2, pp. 464–472, 2021.
[29] A. Neto and J. J. Lee, "Ultrawide-band properties of long slot arrays," *IEEE Trans. Antennas Propag.*, vol. 54, no. 2, pp. 534–543, Feb. 2006.
[30] D. M. Pozar, "A relation between the active input impedance and the active element pattern of a phased array," *IEEE Trans. Antennas Propag.*, vol. 51, no. 9, pp. 2486–2489, Sep. 2003.
[31] M. Ng Mou Kehn, M. V. Ivashina, P.-S. Kildal, and R. Maaskant, "Definition of unifying decoupling efficiency of different array antennas—Case study of dense focal plane array feed for parabolic reflector," *AEU Int. J. Electron. Commun.*, vol. 64, no. 5, pp. 403–412, 2010.
[32] S. Stein, "On cross coupling in multiple-beam antennas," *IRE Trans. Antennas Propag.*, vol. 10, no. 5, pp. 548–557, Sep. 1962.
[33] D. M. Pozar, *Microwave Engineering*, 4th ed. Hoboken, NJ, USA: Wiley, 2011.
[34] A. Ludwig, "The definition of cross polarization," *IEEE Trans. Antennas Propag.*, vol. 21, no. 1, pp. 116–119, Jan. 1973.

VIGNESH MANOHAR (Member, IEEE) received the bachelor's degree in electronics and telecommunication engineering from the University of Mumbai in 2013, and the M.S. and Ph.D. degrees in electrical and computer Engineering from University of California at Los Angeles in 2016 and 2020, respectively.

He is currently a Postdoctoral Associate with the Department of Electrical and Computer Engineering, Florida International University. His research area focuses on the development of wideband antenna arrays, and deployable high gain aperture antennas for small satellite platforms. He was a recipient of the Outstanding Masters Thesis Award in the Physical and Wave Electronics for the year 2016 and the Henry Samueli Excellence in Teaching award in 2020. He received an Honorable Mention in the 2017 and 2018 Altair FEKO student competition for his work on stepped reflectors and characterization of planar near-field antenna measurements. He was also the recipient of the 2019 IEEE Electromagnetic Theory Symposium Young Scientist Award for his work on umbrella reflector antenna characterization.

SHUBHENDU BHARDWAJ (Member, IEEE) received the B.Tech. degree (*summa cum laude*) in electronics engineering from IIT Dhanbad, Dhanbad, India, in 2004, the M.S. degree from UCLA, Los Angeles, CA, USA, in 2012, and the Ph.D. degree from The Ohio State University, Columbus, OH, USA, in 2017. From 2008 to 2010, he worked with Samsung India Software Operations, Bengaluru, India. Since 2017, he has been an Assistant Professor with the Electrical and Computer Engineering Department, Florida International University, Miami, FL, USA. He is currently working on different topics within electromagnetics, including computational electromagnetics, power harvesting, terahertz devices, slow wave structures, and sub-mm-wave/terahertz antennas. He was a recipient of best student paper awards at URSI-GASS-2017, IEEE-iWat-2017, and IEEE-AMTA-2015. His paper also received second place at the Student Paper Competition at AMTA-2014 and HonorableMentions at APS-2014 and 2015.

SATHEESH BOJJA VENKATAKRISHNAN (Senior Member, IEEE) was born in Tiruchirappalli, India, in 1987. He received the bachelor's degree in electronics and communication engineering from the National Institute of Technology, Tiruchirappalli, in 2009, and the M.S. and Ph.D. degrees in electrical engineering from the Ohio State University, Columbus, OH, USA, in 2017.

He was a Scientist for DRDO, India, from 2009 to 2013, working on the development and implementation of active electronic steerable antennas. He is currently a Research Assistant Professor with Electrical and Computer Engineering, Florida International University. He is also working on Simultaneous Transmit and Receive System, to improve the spectral efficiency. His current research includes receiver design for communication circuits, RF systems, and digital signal processing using FPGAs. He was a recipient of the IEEE Electromagnetic Theory Symposium Young Scientist Award in 2019. He won the 2nd Prize in International Union of Radio Science General Assembly and Scientific Symposium (URSI-GASS) student paper competition held at Montreal, Canada, in August 2017. He also received Honorable Mention in the student paper competition at the IEEE Antenna and Propagation Symposium (AP-S/URSI) in 2015 and 2016, and the Student Fellowship Travel Grant Award at the U.S. National Committee for the International Union of Radio Science (USNC–URSI) in 2016 and 2017. He has been a Phi Kappa Phi Member since 2015.

JOHN L. VOLAKIS (Fellow, IEEE) was born in Chios, Greece, in May 13, 1956, and immigrated to USA, in 1973. He received the B.E. degree (*summa cum laude*) from Youngstown State University, Youngstown, OH, USA, in 1978, and the M.Sc. and Ph.D. degrees from The Ohio State University, Columbus, OH, in 1979 and 1982, respectively.

He started his career with Rockwell International (currently, Boeing) from 1982 to 1984. In 1984, he was appointed as an Assistant Professor with The University of Michigan, Ann Arbor, MI, USA, becoming a Full Professor in 1994. He also served as the Director of the Radiation Laboratory from 1998 to 2000. From January 2003 to August 2017, he was the Roy and Lois Chope Chair Professor of Engineering with the Ohio State University and served as the Director of the ElectroScience Laboratory from 2003 to 2016. Effective August 2017, he is the Dean of the College of Engineering and Computing and a Professor with the Electrical and Computer Engineering, Florida International University. Over the years, he carried out research in antennas, wireless communications and propagation, computational methods, electromagnetic compatibility and interference, design optimization, RF materials, multiphysics engineering, millimeter waves, terahertz, and medical sensing. His publications include eight books, 430 journal papers, nearly 900 conference papers, 29 book chapters, and 25 patents/disclosures. His coauthored books are: *Approximate Boundary Conditions in Electromagnetics*, 1995; *Finite Element Methods for Electromagnetics*, 1998; *Antenna Engineering Handbook*, 4th Edition, 2007; *Small Antennas*, 2010; and *Integral Equation Methods for Electromagnetics*, 2011. He has graduated/mentored 95 doctoral students/postdoctorals with 43 of them receiving best paper awards at conferences. His service to professional societies include: 2004 President of the IEEE Antennas and Propagation Society (2004), Chair of USNC/URSI Commission B (2015–2017), twice the General Chair of the IEEE Antennas and Propagation Symposium, IEEE APS Distinguished Lecturer, IEEE APS Fellows Committee Chair, IEEE-Wide Fellows Committee Member and an associate editor of several journals. He was listed by ISI among the top 250 most referenced authors in 2004. Among his awards are: The University of Michigan College of Engineering Research Excellence Award in 1993, the Scott Award from The Ohio State University College of Engineering for Outstanding Academic Achievement in 2011, the IEEE AP Society C.-T. Tai Teaching Excellence Award in 2011, the IEEE Henning Mentoring Award in 2013, the IEEE Antennas and Propagation Distinguished Achievement Award in 2014, The Ohio State University Distinguished Scholar Award in 2016, and The Ohio State University ElectroScience George Sinclair Award in 2017, and URSI Booker Gold Medal in 2020. He is a Fellow of ACES and URSI.